IEEE Access
Multidisciplinary ⋮ Rapid Review ⋮ Open Access Journal

Received April 14, 2021, accepted April 20, 2021, date of publication April 23, 2021, date of current version April 30, 2021.

Digital Object Identifier 10.1109/ACCESS.2021.3075212

Prediction of Hydration Heat of Mass Concrete Based on the SVR Model

DUNWEN LIU, WANMAO ZHANG, YU TANG, AND YINGHUA JIAN
School of Resources and Safety Engineering, Central South University, Changsha 410083, China

Corresponding author: Yu Tang (tangyu9433@163.com)

This work was supported by the Postdoctoral Science Foundation of Central South University through the Initiation Fund for Postdoctoral Research under Grant 228697.

ABSTRACT Thermal cracking in pile caps caused by concrete hydration heat will affect the safety and durability of long-span cable-stayed bridges. Therefore, effective prediction and control of concrete bridges hydration heat has been a challenging problem. In this study, the temperature of hydration heat in mass concrete pile caps belonging to a long-span cable-stayed bridge in China were monitored. Then, we adopt support vector machine regression (SVR) to establish the correlation between influencing variables and the temperature of hydration heat. The monitoring data are used to train to realize the short-term prediction of concrete temperature. The predicted results show that the SVR has a high accuracy, and the deviation between the prediction results and the measured values is quite small. The prediction performance of SVR for temperature of hydration heat of mass concrete is obviously better than that of BP neural network. The SVR prediction model can predict the temperature of 2-3 days with high accuracy. Based on the prediction results, temperature control method can be taken in advance to reduce the possibility of thermal cracks, which is of great significance for the safety and durability of actual engineering construction.

INDEX TERMS Mass concrete, heat of hydration, support vector machine, regression model, temperature prediction.

I. INTRODUCTION

As the foundation of national economic development, the construction quality of bridge projects is influenced by various factors. The pile caps are the key structures for large-span bridges, where temperature changes during concrete hydration may lead to thermal cracking [1]. The expansion and contraction caused by thermal actions contribute to the development of tensile stress in concrete [2]. When the stress exceeds the concrete tensile strength, the thermal cracks will generate [3], [4], affecting the performance, serviceability, and durability of the concrete structure [5], [6]. The number of large-span bridges under construction in China is steady increasing, the amount of mass concrete pile cap is also increasing. Therefore, the study on hydration heat of mass concrete is significant in preventing thermal cracks and ensuring the quality pile caps.

Calculation of the temperatures of concrete hydration heat is required before the construction of mass concrete on bridges. However, the existing bridge design codes have no provisions for calculating the temperature field of hydration heat. Theoretical studies on the heat of hydration of mass concrete began in the 1930s with the construction of the Hoover Dam in the United States. After nearly a century of development, many studies have been conducted on the thermal cracks control regarding cement type [7], concrete type [8]–[10], curing methods [11], mixing ratios [12], and admixtures [13], etc. on the heat of hydration of concrete [14], [15]. However, most of the studies were conducted in the laboratory under semi-adiabatic conditions, few of them were applied to practical engineering. Among them, a large number of experts and scholars, such as Zheng and Xu *et al.*, had compared the finite element analysis results with the field measurements by establishing a finite element model of the heat of hydration of mass concrete [16]–[18]. Tasri *et al.* studied the arrangement and related parameters of cooling water pipes commonly used in mass concrete projects based on the finite element method [19]–[21]. Cha *et al.* introduced a new temperature and stress monitoring device for mass concrete crack control [22]–[24]. Pepe *et al.* proposed new numerical procedures and models to study the temperature and stress fields of mass concrete based on the existing finite

The associate editor coordinating the review of this manuscript and approving it for publication was Jon Atli Benediktsson.

element simulations in conjunction with the development of computational methods [25]–[28].

Above scholars have studied the development law of heat of hydration of mass concrete based on theoretical analysis and field tests, and proposed targeted temperature control measures. However, further research is still needed for real-time prediction of temperature of hydration heat in mass concrete during construction. In the aspects of temperature prediction, Trtnik *et al.* used artificial neural networks to predict the early adiabatic temperature rise of concrete by fields monitoring the concrete structure temperature [29]. However, artificial neural networks have slow convergence speed, poor generalization performance, and sometimes overfitting problems. Subasi *et al.* predicted the early temperature of hydration heat based on an adaptive neuro-fuzzy inference system, and the prediction results were better than those of artificial neural networks [30]. Previous studies only predicted the adiabatic temperature rise of cement and the maximum temperature of concrete. However, they did not achieve real-time temperature prediction of mass concrete, which was not enough to guide the thermal control design. In recent years, with the advancement of computer technology, machine learning methods such as support vector machines (SVM) have been gradually applied to the bridge engineering [31], [32]. SVM provide strong support for the study of factors influencing the hydration heat of mass concrete and regression prediction of temperature development, etc. SVM is a new and effective method to improve the generalization performance, which can reach the global minimum. SVM achieves good generalization ability by adopting the principle of structural risk minimization induction. It aims to minimize the boundary of model generalization error, rather than minimizing the error of the training data only. It has the ability to avoid overtraining and has better generalization capability than artificial neural network models. Some applications of SVM in civil engineering problems include concrete workability prediction [33], slope reliability analysis [34], settlement studies of shallow foundations [35], seismic liquefaction assessment [36], and prediction of tunnel water gushing [37]. In addition, relevance vector machine (RVM) is a nonlinear relation machine learning method which is popular in recent years [38]–[40]. It has the advantages of high precision, high efficiency and adaptability to small samples. However, when the input sample dimension is large, the learning efficiency of RVM will be reduced and the computing cost will be increased. Compared with SVM, the main disadvantage of relevance vector machine is the relatively long training time. In this study, SVM is applied to predict the temperatures of concrete hydration heat for the first time and compared with the prediction accuracy of BP neural networks applied by previous researchers.

Under the complex construction conditions and higher quality requirements, it is important to avoid thermal cracks in mass concrete. In this study, in order to ensure the concrete construction quality of pile cap in a bridge project in China, the concrete mix ratio is optimized to reduce the adiabatic temperature rise before construction. The temperature control measures are carried out from the aspects of concrete entering mold temperature, cooling water circulation system, curing water temperature and so on. What is more, the temperature sensors and environment monitoring devices were pre-installed inside the pile cap to monitor the concrete temperature, ambient temperature and cooling water temperature in real time. Therefore, the monitoring data are trained based on SVM algorithm to achieve short-term prediction of concrete temperature. The prediction results of SVM and BP neural network are compared to verify their prediction performance.

II. THEORETICAL BASIS

A. SUPPORT VECTOR MACHINES

Support vector machine (SVM) is a new machine learning method based on the statistical learning theory (STL) created by Vapnik. The statistical learning theory uses the structural risk minimization (SRM) criterion to minimize the structural risk. While minimizing the sample point error, it improves the generalization ability of the model without the limitation of data dimensionality [41].

In order to solve the regression fitting problem by SVM, Vapnik *et al.* introduced the ε-insensitive loss function on the basis of SVM classification to obtain the support vector machine for regression (SVR), and achieved good performance and results. The basic concept of SVR is to find an optimal classification surface that minimizes the error of all training samples from the optimal classification surface.

Without loss of generality, let the training set sample pair containing l samples be $\{(x_i, y_i), i = 1, 2, \ldots, l\}$, where $x_i (x_i \in R_d)$ is the input column vector of the ith training sample, $x_i = [x_i^1, x_i^2, \ldots, x_i^d]^T$, $y_i \in R$ is the corresponding output value.

Let the linear regression function established in the high-dimensional feature space be

$$f(x) = \omega \Phi(x) + b \tag{1}$$

where $\Phi(x)$ is a nonlinear mapping function.

Define ε as the linear insensitive loss function. FIGURE 1 illustrates ε insensitive loss function setting to given data in SVM, and it is also represented by the following equation:

$$L(f(x), y, \epsilon) = \begin{cases} 0, & |y - f(x)| \leq \epsilon \\ |y - f(x)| - \epsilon, & |y - f(x)| > \epsilon \end{cases} \tag{2}$$

where $f(x)$ is the predicted value returned by the regression function; y is the corresponding true value. That is, it means that if the difference between $f(x)$ and y is less than or equal to ε, the loss is equal to 0.

Similar to the SVM classification case, the relaxation variables ξ_i and ξ_i^* are introduced and the above problem of

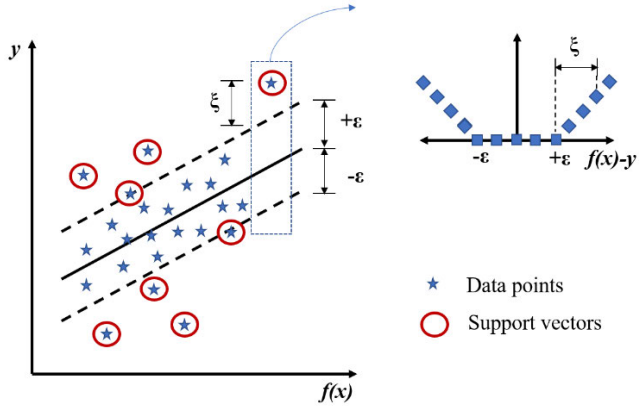

FIGURE 1. ε **insensitive loss function setting for SVM in regression.**

finding ω, b is described in mathematical terms:

$$\begin{cases} min \frac{1}{2}\|\omega\|^2 + C\sum_{i=1}^{l}\left(\xi_i + \xi_i^*\right) \\ s.t. \begin{cases} y_i - \omega\Phi\left(x_i\right) - b \le \epsilon + \xi_i \\ -y_i + \omega\Phi\left(x_i\right) + b \le \epsilon + \xi_i^* \\ \xi_i \ge 0, \xi_i^* \ge 0 \end{cases} \end{cases} \quad , i = 1, 2, \ldots, l \tag{3}$$

where C is the penalty factor, the larger C means the greater the penalty for samples with training error greater than ε. ε specifies the error requirement of the regression function, and the smaller ε means the smaller the error of the regression function [42], [43].

When solving equation (3), the Largrange function is also introduced and converted to the dual form through equation (4).

$$\begin{cases} \underset{\alpha,\,\alpha^*}{max} \left[-\frac{1}{2}\sum_{i=1}^{l}\sum_{j=1}^{l}\left(\alpha_i - \alpha_i^*\right)\left(\alpha_i - \alpha_j^*\right)K\left(x_i, x_j\right)\right. \\ \left. -\sum_{i=1}^{l}\left(\alpha_i + \alpha_i^*\right)\varepsilon + \sum_{i=1}^{l}\left(\alpha_i - \alpha_i^*\right)y_i\right] \\ s.t. \begin{cases} \sum_{i=1}^{l}\left(\alpha_i - \alpha_i^*\right) y_i = 0 \\ 0 \le \alpha_i \le C \\ 0 \le \alpha_i^* \le C \end{cases} \end{cases} \tag{4}$$

where $K(x_i, y_i) = \Phi(x_i)\Phi(x_j)$ is the kernel function.

Let the optimal solution of the solution equation be, then $\alpha = [\alpha_1, \alpha_2, \ldots, \alpha_l]$ and $\alpha^* = [\alpha_1^*, \alpha_2^*, \ldots, \alpha_l^*]$, then we have

$$\omega^* = \sum_{i=1}^{l}\left(\alpha_i - \alpha_i^*\right)\Phi\left(x_i\right) \tag{5}$$

$$b^* = \frac{1}{N_{nsv}}\left\{\begin{array}{c} \sum_{0<\alpha_i<C}\left[y_i - \sum_{x_i \in SV}\left(\alpha_i - \alpha_i^*\right)\right. \\ \left. K\left(x_i, x_j\right) - \varepsilon\right] \\ +\sum_{0<\alpha_i<C}\left[y_i - \sum_{x_j \in SV}\left(\alpha_j - \alpha_j^*\right)\right. \\ \left. K\left(x_i, x_j\right) + \varepsilon\right] \end{array}\right\} \tag{6}$$

where N_{nsv} is the number of support vectors. Thus, the regression function is

$$\begin{aligned} f\left(x\right) &= \omega^*\Phi\left(x\right) + b^* = \sum_{i=1}^{l}\left(\alpha_i - \alpha_i^*\right)\Phi\left(x_i\right)\Phi\left(x\right) + b^* \\ &= \sum_{i=1}^{l}\left(\alpha_i - \alpha_i^*\right)K\left(x_i, x\right) + b^* \end{aligned} \tag{7}$$

where only some of the parameters $(\alpha_i - \alpha_i^*)$ are not zero, and their corresponding samples x_i are the support vectors in the problem.

The prediction of the testing set is performed by using the regression function. The mean squared error E and squared correlation coefficient R^2 of the testing set are recorded, and the specific formulas are:

$$E = \frac{1}{l}\sum_{i=1}^{l}\left(\hat{y}_i - y_i\right)^2 \tag{8}$$

$$R^2 = \frac{\left(l\sum_{i=1}^{l}\hat{y}_i y_i - \sum_{i=1}^{l}\hat{y}_i\sum_{i=1}^{l}y_i\right)^2}{\left(l\sum_{i=1}^{l}\hat{y}_i^2 - \left(\sum_{i=1}^{l}\hat{y}_i\right)^2\right)\left(l\sum_{i=1}^{l}y_i^2 - \left(\sum_{i=1}^{l}y_i\right)^2\right)} \tag{9}$$

where l is the number of samples in the testing set; $y_i(i = 1, 2, \ldots, l)$ is the true value of the ith sample. $\hat{y}_i(i = 1, 2, \ldots, l)$ is the predicted value of the ith sample.

The established regression model is evaluated based on E and R^2. If the performance does not meet the requirements well, the model is re-modeled by changing the kernel function or other model parameters until the performance meets the requirement.

III. ENGINEERING APPLICATION

A. ENGINEERING BACKGROUND

The main bridge is 1070m long, with a span of (69+176+580+176+69) m. The bridge is a double-tower, double-cable hybrid girder cable-stayed bridge, its elevation is shown in Figure 2. The main pile cap is made of C40 concrete, the shape of the pile cap is designed into an oval shape, taking into account the influence of structural force and water flow. The plane size of the bearing platform is 26.5m (along the bridge) × 68m (across the bridge), the thickness of the pile cap is 6m, and the concrete pouring volume is 9720m^3.

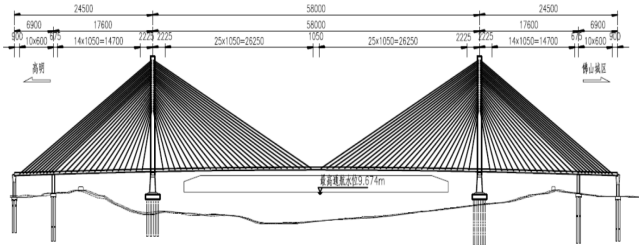

FIGURE 2. **Schematic diagram of the bridge elevation arrangement (unit: cm).**

To meet the mechanical properties and durability design requirements of concrete, reduce thermal cracks of mass concrete. Based on the design requirements of concrete ratio, the pile cap increased the amount of mineral admixture to delay and reduce the concrete hydration temperature rise [44]. On the premise of meeting the work performance, reduce the sand rate as much as possible to improve the volume stability of concrete and reduce the dry shrinkage rate of concrete. Under the premise of matching the construction

TABLE 1. Adiabatic temperature rise comparison test scheme.

Test number	Project site	Compounding parameters						Maximum adiabatic temperature rise (℃)
		Water to glue ratio	Total adhesive material	Fly ash mixing amount	Slag powder mixing amount	Additive dosing	Sand rate	
F35P15-1	Main bridge bearing	0.40	380	35%	15%	1.3%	39%	46.35
F35P15-2		0.38	400			1.0%	38%	48.89
F45P25-1		0.40	380	45%	25%	1.3%	39%	39.62
F45P25-2		0.38	400			1.0%	38%	40.70

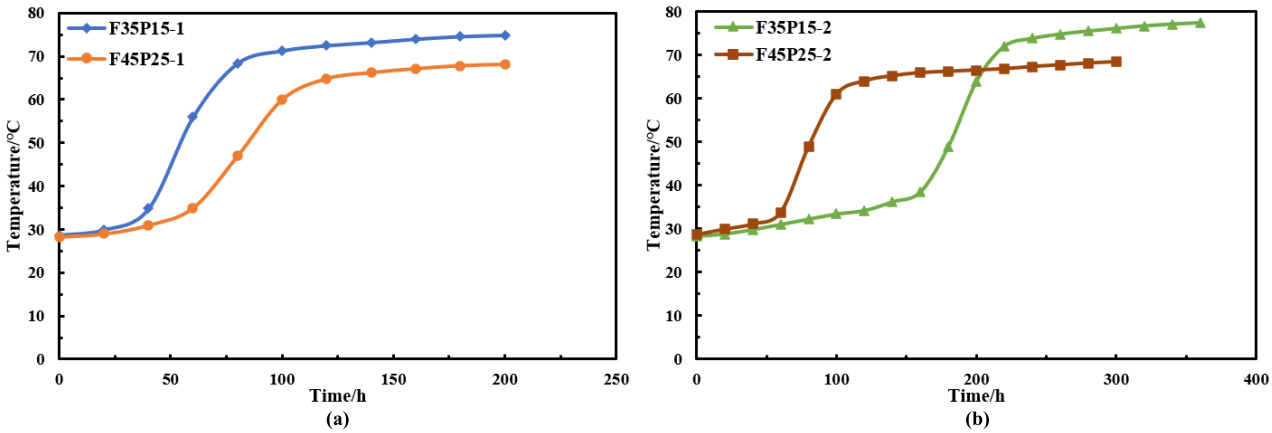

FIGURE 3. Adiabatic temperature rise curve of concrete with different ratio design. (a) Water-cement ratio 0.40, total cementitious material 380kg/m^3; (b) Water-cement ratio 0.38, total cementitious material 400kg/m^3.

TABLE 2. Recommended concrete ratio design parameters for bearing platform.

Project site	Compounding parameters					
	Water to glue ratio	Total adhesive material	Fly ash mixing amount	Slag powder mixing amount	Additive dosing	Sand rate
Main bridge bearing C40	0.38	400	45%	25%	1.0%	38%

process, try to extend the concrete setting time [45], [46]. To prevent the cracking problem caused by the temperature difference and dry shrinkage of mass concrete, the adiabatic temperature rise test of concrete with different water-cement ratio, different amount of total cement and different amount of mineral admixtures were carried out respectively. The test scheme is shown in Table 1.

The concrete temperature of the above was continuously monitored, and the adiabatic temperature rise curves of concrete with different ratio designs were obtained as shown in Figure 3.

According to experimental data, the concrete maximum temperature rise decreases with the increase of the content of mineral admixture. In the same case of cementitious materials, the content of admixture increases by 20%, and the adiabatic temperature rise decreases by 14.5%−16.8%. The maximum temperature rise of concrete increases with the increase of the total cementitious material. Under the premise of the increase of the total cementitious material by 20kg, the adiabatic temperature rise increases by 2.7%∼5.5%. According to the experimental conclusion, the concrete mix ratio of the pile cap is shown in TABLE 2, and the maximum adiabatic temperature rise at this time is 40.7°.

According to the field construction conditions, the following temperature control measures were taken during construction to ensure the quality of the mass concrete construction of the pile cap.

(1) The pile cap was poured in layers and the suitable pouring thickness was designed. The concrete was poured in 3 layers, the first layer was 1.5m with a volume of 2430m^3; the second layer was 2m with a volume of 3240m^3; the third layer was 2.5m with a volume of 4050m^3. After each layer was poured, the next layer was poured about 14 days later.

(2) Laid out the cooling water pipe and set the appropriate vertical and horizontal spacing. The cooling water pipe was arranged in four layers, the first layer of concrete was arranged at 0.8m from the sealing concrete; the second layer of concrete was arranged at 1.0m position from the top of the first layer; the third layer of concrete was arranged at 0.5m and 1.5m from the top of the second layer. The horizontal spacing of each cooling pipe was 1.5m, and the upper and lower layers of cooling pipes were staggered longitudinally and horizontally, and they would be slurry treated after use.

(3) Implemented water storage and heat preservation on the surface of pile cap. In order to ensure that the temperature difference between inside and outside of the concrete in the pile cap was not more than 25°, after the concrete in the pile cap was poured and the initial setting was completed, the circulating water at the outlet of the cooling water pipe was used for timely water storage and heat preservation. On the one hand, the concrete surface can be kept warm to avoid excessive temperature difference between inside and outside, and on the other hand, the concrete can be bearing the concrete for nourishment.

B. DATA COLLECTION

In order to realize the informationized temperature control construction and timely adjust the temperature control measures such as water pipe parameters in abnormal situations, thermistor sensors with a sensitivity of 0.1 °C were arranged inside the pile cap [47]. And a wireless automatic temperature acquisition box was adopted for data acquisition, transmission and storage. The physical layout diagram of the sensors in the field is shown in Figure 4. When the main pile cap concrete was poured, 2 layers of measurement points (layer number A, B, C and D respectively) were placed in the first and second layers, and 3 layers of measurement points (layer number E, F and G respectively) were placed in the third layer. 14 temperature measurement points were placed in each layer, and the ambient temperature, concrete mold temperature and the temperature of cooling pipe inlet and outlet were monitored at the same time, totaling 102 measurement points. The measurement points were arranged within 1/4 of the pile cap and along the horizontal and vertical directions. The plane layout and number of the measuring points are shown in Figure 5. The concrete temperature was monitored in real time, and the observation period was generally once every 1 hour before the peak, and once every 2 hours after the peak, until the basic stability.

Considering the time difference of concrete construction on the pile cap, the existence of a certain time difference of cement hydration reaction, and environment factors, temperature monitoring data would inevitably appear errors or data loss. Therefore, the temperature of the pile cap concrete was regionalized according to the relative position of the sensor, which could be divided into the central area (Q1), the sub-central area (Q2) and the edge area (Q3). So the average value of the measurement points in the area represented the temperature of the area.

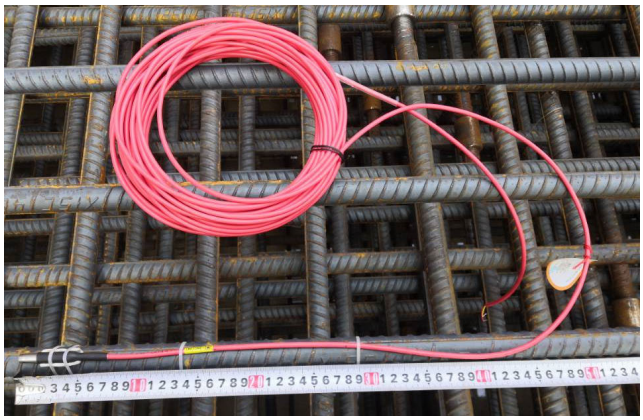

FIGURE 4. Physical diagram of sensor site arrangement.

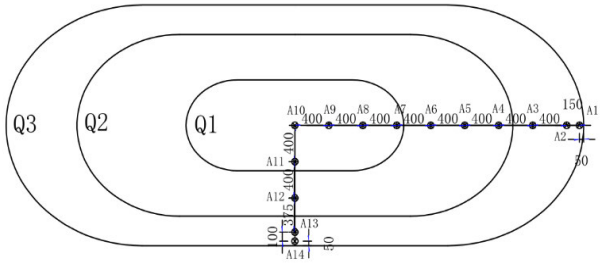

FIGURE 5. Schematic layout of measurement points (unit: cm).

C. THE SVR TEMPERATURE PREDICTION MODEL

1) INFLUENCING FACTORS OF HYDRATION HEAT

The temperature field of mass concrete in pile cap is influenced by the interaction of internal and external factors such as hydration heat state and construction environment. The temperature difference will cause temperature stress in structure [48]. The hydration heat state of concrete, the ambient temperature and the water temperature of the pipe cooling system also change constantly with the construction process. The comprehensive influence of these factors lead to the nonlinear temperature field of mass concrete structure which change with time [49], [25]. The internal factors that affect the temperature field of mass concrete mainly include concrete mixture ratio, additive type, fly ash content, structure size of pile cap and so on. External factors mainly include insulation measures, solar radiation, construction site wind speed, pipe cooling system layout, environmental temperature, etc. And the mass concrete in occasional circumstances may also encounter fire, wind and rain, hail and other harsh conditions. Concrete has the characteristics of low thermal conductivity and poor heat transfer ability, which leads to the slow change of temperature field and nonlinear temperature state of different parts.

The concrete of the pile cap is designed with the same proportion, and the types of additives and fly ash admixture are the same. Therefore, the internal factors affecting the temperature field of mass concrete were not considered. For the external factors, combined with the site climate monitoring,

TABLE 3. Sample data.

Number	Influencing factors(x_i)			Measured temperature(y_i)		
	Pouring time/h	Ambient temperature/°C	Cooling water temperature/°C	The edge area temperature/°C	The sub-central area temperature/°C	The center area temperature/°C
1	0	27.0	26	28.0	28.1	28.2
2	2	26.7	26	28.5	28.7	28.7
3	4	25.6	24.6	28.9	29.1	28.9
4	6	28.4	32.6	29.0	29.5	29.8
5	8	33.7	31.2	29.6	30.2	30.7
…	…	…	…	…	…	…
68	134	25.0	-	38.3	41.1	42.4
69	136	24.6	-	38.1	40.9	42.2
70	138	24.1	-	38.0	40.6	41.9
71	140	23.8	-	37.8	40.4	41.7
72	142	23.2	-	37.6	40.2	41.6
73	144	22.8	-	37.3	40	41.4

the influence of main factors of hydration heat temperature was considered.

2) TRAINING AND TESTING

To evaluate the influence of concrete casting time, ambient temperature and cooling water temperature on the temperature of hydration heat in mass concrete. Considering small sample and multiple factors, the SVR model is adopted. The day before the monitoring data is selected as the training sample from the completion of concrete casting to the temperature to be predicted, the temperature data of that day is the prediction samples. The sample data are shown in TABLE 3. The program has been written in the Matlab language to establish the SVR prediction model. The model construction process is shown in Figure. 6. In addition, since the on-site tube cooling system was shut down when the temperature reached the peak, the temperature prediction after the peak did not need to consider the effect of cooling water.

$T = \{(x_i, y_i), i = 1, 2, \ldots, l\}$, where $x_i (x_i \in R_d)$ was the influence factor of the ith training sample, including the concrete pouring time, ambient temperature and cooling water temperature, and $y_i \in R$ is the corresponding concrete temperature in the pile cap area.

3) REGRESSION MODELS

For the common kernel function of SVM, a large number of studies show that the linear kernel function and sigmoid kernel function corresponding to the low accuracy. The RBF kernel function and polynomial kernel function corresponding training set are quite accuracy. However, considering from

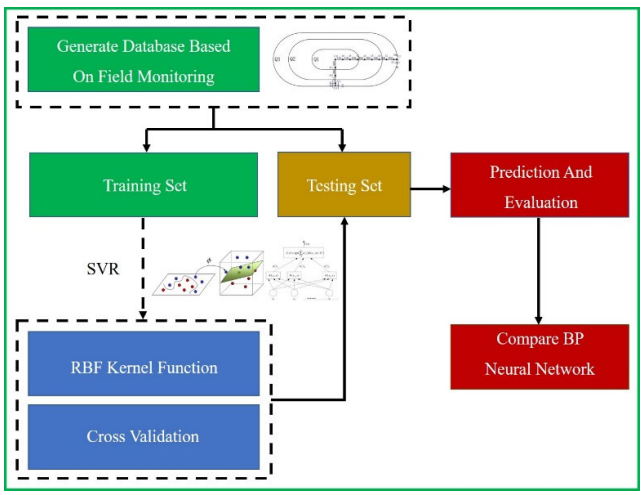

FIGURE 6. SVR model construction process.

the generalization ability of the model, the measure of the prediction accuracy of the testing set at the same time, the corresponding model of RBF kernel function is the best performance [50], [51]. In the calculation of concrete hydration heat prediction analysis for pile cap, the radial basis kernel function (RBF) $K(x_i, x) = exp(-\|x_i - x\|/\sigma^2)$ was found to have the highest computational accuracy by comparison. Therefore, according to the RBF kernel function, this study adopted the cross-validation and grid search method to find the best penalty factor C and variance g in the kernel function. And set the insensitivity factor $\varepsilon = 10^{-5}$ to achieve the creation and training of the SVR model according to equation (3).

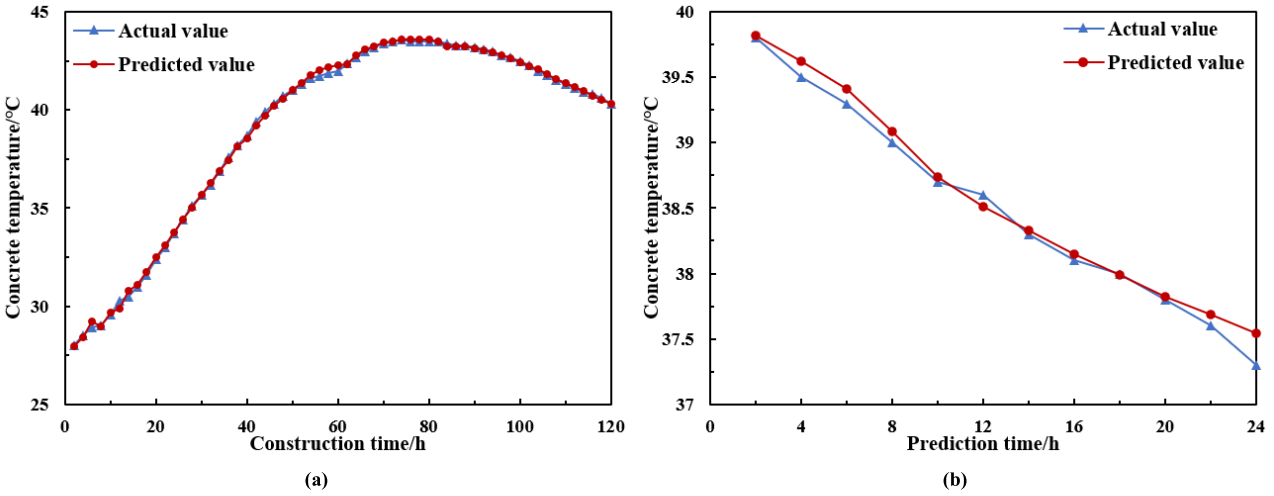

FIGURE 7. Comparison of prediction results in Q1 area. (a) Training set; (b) Testing set.

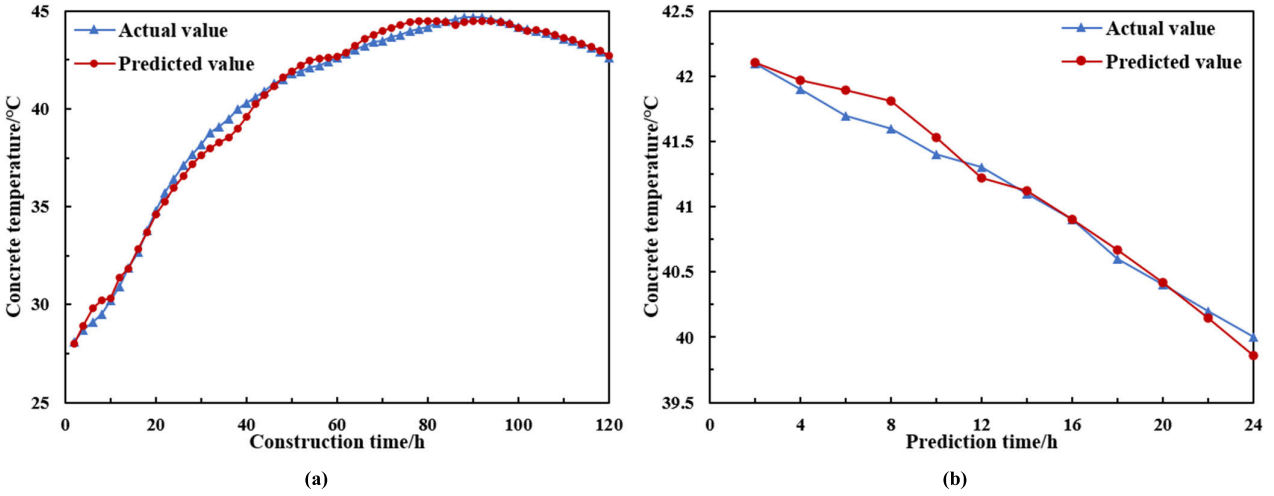

FIGURE 8. Comparison of prediction results in Q2 area. (a) Training set; (b) Testing set.

IV. RESULTS AND DISCUSSION

A. THE SVR PREDICTION RESULTS

The SVR model is used to simulate and predict the temperatures of the center layer measurement point (No. A) of the first layer of concrete in the pile cap by single-step forecasting method. The measured temperature samples of the first 7 days are taken as the training set and the samples of the 8th day are taken as the testing set. The temperature prediction results of the training and testing set for the center (Q1 area.), sub-center (Q2 area.) and edge (Q3 area.) areas are shown in Figure 7, Figure 8, and Figure 9.

The mean square error *(MSE)* and squared correlation coefficient (R^2) of the training set and the testing set can be obtained from the above calculation formula. The results are shown in Table 4.

Comparing the MSE and R^2 calculated from the training and testing set in each area of the pile cap in TABLE 4. The MSE of both training and testing set are very small, which can reach 10^{-3}. The R^2 of the training and testing sets can reach above 0.99 and 0.98, respectively. This indicates that

TABLE 4. Mean square error E and squared correlation coefficient R^2 of training set and testing set.

The cap area	Training set		Testing set	
	Mean square error E	Squared correlation coefficient R^2	Mean square error E	Squared correlation coefficient R^2
Q1 area	0.002898	0.99924	0.001537	0.98967
Q2 area	0.002113	0.99371	0.001686	0.98693
Q3 area	0.001144	0.99667	0.004558	0.98155

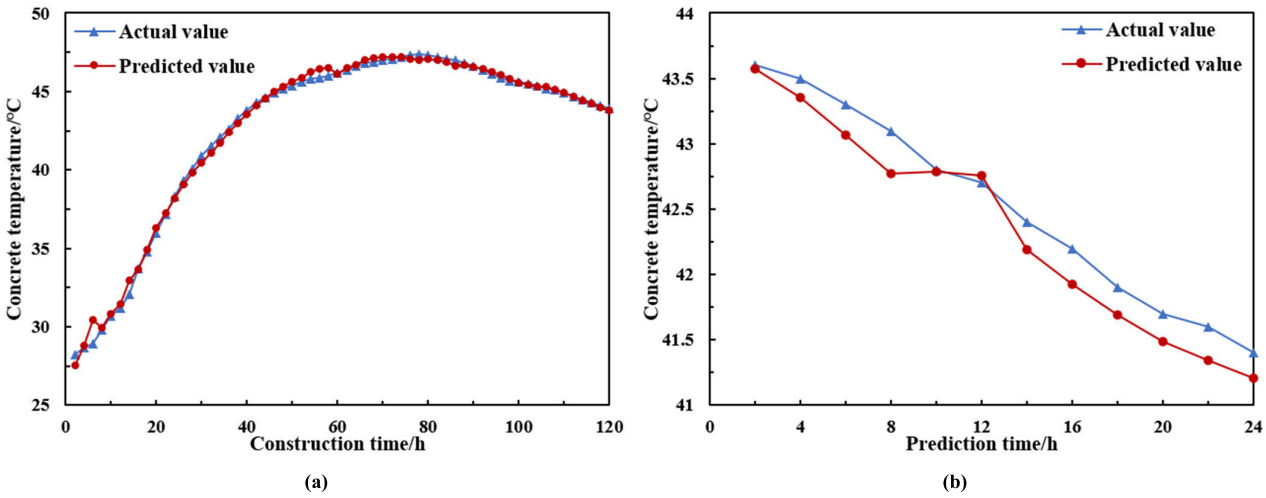

FIGURE 9. Comparison of prediction results in Q3 area. (a) Training set; (b) Testing set.

the deviation between the predicted results and the measured values is small, and the SVR model can achieve a high accuracy prediction temperature of hydration heat.

By comparing the MSE and the R^2 of the prediction results for the central, sub-central and edge areas, it is found that the training and testing results of the SVR for the edge area are better than those for the sub-central and central area. This is because among the various influencing factors of the training samples, the influence of ambient temperature on the concrete edge of the pile cap is more significant.

B. PARAMETER ANALYSIS

For the RBF kernel function selected in this study, the results of the optimal parameters penalty factor C and kernel function variance g obtained by cross-validation and grid search method are shown in Table 5. Then, the model was trained based on the optimal parameters. When the model performance is the same, in order to reduce the calculation time, the parameter combinations with smaller C value is selected. This is because the larger C value is, the more support vectors are obtained and the more calculation time is needed.

TABLE 5. The best parameters C and g calculated by the cross-validation method.

The cap area	Penalty factor C	Kernel function variance g
Q1 area	2.8284	1
Q2 area	362.0387	0.0625
Q3 area	11.3137	0.5

Many studies showed that the model corresponding to the RBF kernel function had the best performance. Therefore, in this work, RBF function is adopted to train SVR. In this process, the values of parameters C and g need to be considered. Intuitively, low value C made the decision surface smooth, while high value C aimed to correctly classify all training samples by giving the model the freedom to choose more samples as support vectors. The parameter g defined how far the impact of a single training sample had reached, with a low value meaning ''far'' and a high value meaning ''close''. The parameter g could be considered as the reciprocal of the radius of the influence of the sample selected by the model support vector.

In this study, the penalty factor C in Q2 area was much larger than that in Q3 area and Q1 area, so the samples in this area needed more support vector numbers in the training process to achieve the ideal training effect. The smaller penalty factor C in Q1 and Q3 made the training result fluctuate less and the curve was smoother. In addition, parameter g in Q2 area was small, indicating that the sample influence radius of the model support vector was larger during training. The above phenomenon was mainly caused by the time difference of concrete pouring on the cap, the large span of pouring range in Q2 area, and the large fluctuation of monitoring data of the temperature sensors in initial stage. At the same time, the concrete temperatures in the construction process were more affected by the adjacent area, which led that the sample training effect in this area was not as good as other areas.

C. MODEL PERFORMANCE EVALUATION

The accuracy of the above mentioned SVR hydration heat temperature prediction model was compared with the neural network-based prediction model. The statistical analysis results of the BP neural network model for the testing samples in the central area of the bearing platform are given in Figure 10. The squared correlation coefficient R^2 based on the prediction results of artificial neural network can only reach 0.2. Compared with the SVR model, the predicted values of the BP neural network model maintain a high prediction accuracy in the first 14 hours. After this period, the accuracy decreases significantly, and the maximum error of prediction

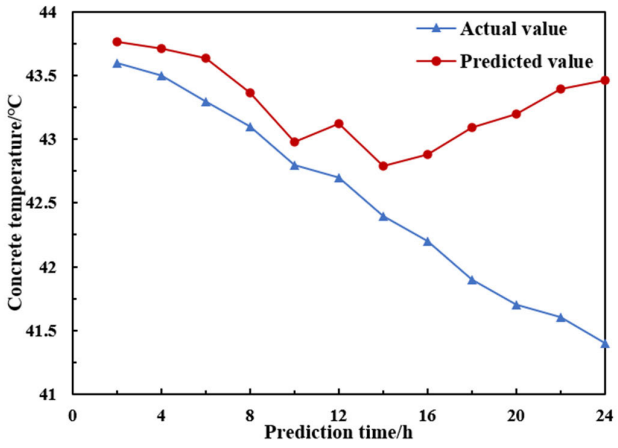

FIGURE 10. Prediction results of BP neural network in central area.

exceeds 2°C, indicating that the BP neural network model has a limited prediction time range for the hydration heat temperature. In order to verify the time range of the established SVR model to predict the temperature more accurately, the measured temperature samples of the first 7 days were taken as the training set. And the monitored temperature samples of the 8th-10th days were taken as the testing set. The temperature prediction results of the central area testing set are shown in FIGURE 11. By analyzing the prediction results of the SVR model on the hydration heat temperature, it can be seen that the prediction accuracy is high within the first 52 hours, the accuracy decreases in the 52-72 hours. The prediction accuracy decreases, but the maximum error of prediction does not exceed 1 °C. In summary, the prediction performance of the SVR model was significantly better than that of the BP neural network model.

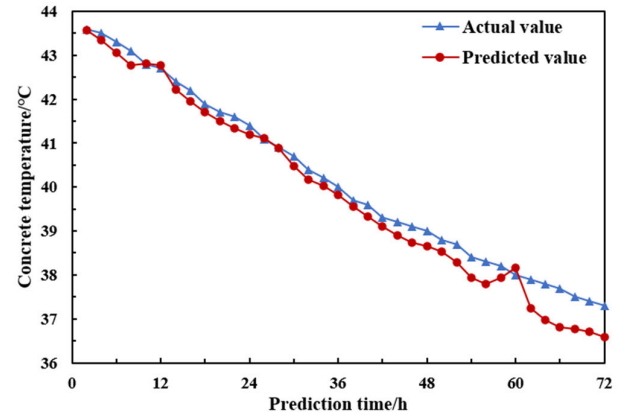

FIGURE 11. Predicted results of SVR in central area.

For this reason, the artificial neural network model was mainly used to study the statistical properties when the sample points tended to infinity, which required the development of a large number of optimal control parameters and a relatively large training database. However, SVR model did not involve the use of probability measure, the law of large numbers and other related knowledge. Computational complexity only depended on the number of support vector. The required size dependence of the training data set was small, which could effectively avoid the dimension disaster. It could overcome the overlearning problem of artificial neural network and greatly simplify the regression problem. SVR these advantages can make it is entirely possible that instead of artificial neural network.

V. CONCLUSION

Based on temperature of hydration heat field tests for pile caps in China, we develop a SVR model to predict temperatures of concrete hydration heat under the influence of concrete pouring time, ambient temperature and cooling water temperature factors. Considering the uncertainty of environmental factors and measurement errors, the measured temperatures of concrete hydration heat are regionalized and used to predict temperatures in the following days. Finally, the prediction results of the SVR model and BP neural network are compared. The main conclusions are drawn from this work as following:

(1) The proposed SVR model can accurately predict the temperatures of concrete hydration heat in pile caps. The SVM prediction results are basically consistent with the measured values, and the maximum error is within 2 °C. In addition, the prediction result of the SVM model is more accurate than that of BP neural network-based prediction model. It identifies that in the case of small samples and short-term temperature prediction, the SVM model can better predict the changing trend of hydration heat for mass concrete with various factors, especially in relation to concrete pouring time.

(2) Comparing the temperature prediction results of each region in the pile cap, the prediction results of central and sub-center areas are more accurate than edge areas. It shows that the influence of ambient temperature around the edge areas of pile cap is more obvious. The relevant parameters results of the SVR model, it was concluded that the model had a better training effect on the samples from the center area and the edge area than the sub-center area.

(3) The SVR model can predict the temperature of hydration heat for 2-3 days with high accuracy. According to prediction results, the construction process can take thermal control measures in advance to avoid harmful cracks. It can provide a scientific and effective method to predict concrete temperature of hydration heat accurately, and also providing a theoretical basis for thermal control of mass concrete.

In this work, the SVR theory is the first time to be used in the prediction of hydration temperature of mass concrete. However, there are some limitations in the method, such as the complex environmental elements. And the solar radiation can be introduced in future studies. While considering too many influencing factors, it is inevitable to have higher requirements for machine learning algorithms. Swarm intelligence algorithms represented by dolphin swarm algorithm

(DSA) and dragonfly algorithm (DA) have good robustness and flexibility, which are the key to solve more complex problems [52]–[56].

REFERENCES

[1] Y. Huang, G. Liu, S. Huang, R. Rao, and C. Hu, "Experimental and finite element investigations on the temperature field of a massive bridge pier caused by the hydration heat of concrete," *Construct. Building Mater.*, vol. 192, pp. 240–252, Dec. 2018, doi: 10.1016/j.conbuildmat.2018.10.128.

[2] I. Chu, S. H. Kwon, M. N. Amin, and J.-K. Kim, "Estimation of temperature effects on autogenous shrinkage of concrete by a new prediction model," *Construct. Building Mater.*, vol. 35, pp. 171–182, Oct. 2012, doi: 10.1016/j.conbuildmat.2012.03.005.

[3] J. H. Yeon, S. Choi, and M. C. Won, "*In situ* measurement of coefficient of thermal expansion in hardening concrete and its effect on thermal stress development," *Construct. Building Mater.*, vol. 38, pp. 306–315, Jan. 2013, doi: 10.1016/j.conbuildmat.2012.07.111.

[4] I. Chu, Y. Lee, M. N. Amin, B.-S. Jang, and J.-K. Kim, "Application of a thermal stress device for the prediction of stresses due to hydration heat in mass concrete structure," *Construct. Building Mater.*, vol. 45, pp. 192–198, Aug. 2013, doi: 10.1016/j.conbuildmat.2013.03.056.

[5] A. Schackow, C. Effting, I. R. Gomes, I. Z. Patruni, F. Vicenzi, and C. Kramel, "Temperature variation in concrete samples due to cement hydration," *Appl. Thermal Eng.*, vol. 103, pp. 1362–1369, Jun. 2016, doi: 10.1016/j.applthermaleng.2016.05.048.

[6] I. F. Dias, J. Oliver, J. V. Lemos, and O. Lloberas-Valls, "Modeling tensile crack propagation in concrete gravity dams via crack-path-field and strain injection techniques," *Eng. Fract. Mech.*, vol. 154, pp. 288–310, Mar. 2016, doi: 10.1016/j.engfracmech.2015.12.028.

[7] E. Hernandez-Bautista, D. P. Bentz, S. Sandoval-Torres, and P. F. D. J. Cano-Barrita, "Numerical simulation of heat and mass transport during hydration of portland cement mortar in semi-adiabatic and steam curing conditions," *Cement Concrete Compos.*, vol. 69, pp. 38–48, May 2016, doi: 10.1016/j.cemconcomp.2015.10.014.

[8] L. A. Sbia, A. Peyvandi, J. Lu, S. U. Abideen, R. R. Weerasiri, A. M. Balachandra, and P. Soroushian, "Study on field thermal curing of ultra-high-performance concrete employing heat of hydration," *ACI Mater. J.*, vol. 114, no. 5, pp. 733–743, Oct. 2017, doi: 10.14359/51689677.

[9] A. S. Tarasov, E. P. Kearsley, A. S. Kolomatskiy, and H. F. Mostert, "Heat evolution due to cement hydration in foamed concrete," *Mag. Concrete Res.*, vol. 62, no. 12, pp. 895–906, Dec. 2010, doi: 10.1680/macr.2010.62.12.895.

[10] T. D. Rupnow, K. Wang, V. R. Schaefer, and P. Tikalsky, "A simple method for characterizing and predicting temperature behavior of ternary cementitious systems," *Construct. Building Mater.*, vol. 25, no. 5, pp. 2290–2297, May 2011, doi: 10.1016/j.conbuildmat.2010.11.022.

[11] X. S. Huo and L. U. Wong, "Experimental study of early-age behavior of high performance concrete deck slabs under different curing methods," *Construct. Building Mater.*, vol. 20, no. 10, pp. 1049–1056, Dec. 2006, doi: 10.1016/j.conbuildmat.2005.04.001.

[12] J. Hu, Z. Ge, and K. Wang, "Influence of cement fineness and water-to-cement ratio on mortar early-age heat of hydration and set times," *Construct. Building Mater.*, vol. 50, pp. 657–663, Jan. 2014, doi: 10.1016/j.conbuildmat.2013.10.011.

[13] H.-M. Woo, C.-Y. Kim, and J. H. Yeon, "Heat of hydration and mechanical properties of mass concrete with high-volume GGBFS replacements," *J. Thermal Anal. Calorimetry*, vol. 132, no. 1, pp. 599–609, Apr. 2018, doi: 10.1007/s10973-017-6914-z.

[14] M. Ismail, A. H. Noruzman, M. A. R. Bhutta, T. O. Yusuf, and I. H. Ogiri, "Effect of vinyl acetate effluent in reducing heat of hydration of concrete," *KSCE J. Civil Eng.*, vol. 20, no. 1, pp. 145–151, Jan. 2016, doi: 10.1007/s12205-015-0045-5.

[15] K.-H. Yang, G.-D. Moon, and Y.-S. Jeon, "Implementing ternary supplementary cementing binder for reduction of the heat of hydration of concrete," *J. Cleaner Prod.*, vol. 112, pp. 845–852, Jan. 2016, doi: 10.1016/j.jclepro.2015.06.022.

[16] Z. Zheng and X. Wei, "Mesoscopic models and numerical simulations of the temperature field and hydration degree in early-age concrete," *Construct. Building Mater.*, vol. 266, no. 1, Jan. 2021, Art. no. 121001, doi: 10.1016/j.conbuildmat.2020.121001.

[17] W. Xu, S. Qiang, Z. Hu, B. Ding, and B. Yang, "Effect of hydration heat inhibitor on thermal stress of hydraulic structures with different thicknesses," *Adv. Civil Eng.*, vol. 2020, no. 5, pp. 1–17, Sep. 2020, doi: 10.1155/2020/5029865.

[18] J. A. Teixeira de Freitas, P. T. Cuong, R. Faria, and M. Azenha, "Modelling of cement hydration in concrete structures with hybrid finite elements," *Finite Elements Anal. Des.*, vol. 77, pp. 16–30, Dec. 2013, doi: 10.1016/j.finel.2013.07.008.

[19] A. Tasri and A. Susilawati, "Effect of cooling water temperature and space between cooling pipes of post-cooling system on temperature and thermal stress in mass concrete," *J. Building Eng.*, vol. 24, no. 10, pp. 09–22, Jul. 2019, doi: 10.1016/j.jobe.2019.100922.

[20] A. Tasri and A. Susilawati, "Effect of material of post-cooling pipes on temperature and thermal stress in mass concrete," *Structures*, vol. 20, pp. 204–212, Aug. 2019, doi: 10.1016/j.istruc.2019.03.015.

[21] P. R. Singh and D. C. Rai, "Effect of piped water cooling on thermal stress in mass concrete at early ages," *J. Eng. Mech.*, vol. 144, no. 3, Mar. 2018, Art. no. 04017183, doi: 10.1061/(ASCE)EM.1943-7889.0001418.

[22] S.-L. Cha, S.-S. Jin, and J.-K. Kim, "Analysis of mass concrete structures with concrete properties by thermal stress device—part II: Verification," *Mag. Concrete Res.*, vol. 72, no. 8, pp. 392–411, Apr. 2020, doi: 10.1680/jmacr.18.00373.

[23] J. Ouyang, X. Chen, Z. Huangfu, C. Lu, D. Huang, and Y. Li, "Application of distributed temperature sensing for cracking control of mass concrete," *Construct. Building Mater.*, vol. 197, pp. 778–791, Feb. 2019, doi: 10.1016/j.conbuildmat.2018.11.221.

[24] G. M. Ji, T. Kanstad, and Ø. Bjøntegaard, "Numerical modelling of field test for crack risk assessment of early age concrete containing fly ash," *Adv. Mater. Sci. Eng.*, vol. 2018, no. 10, pp. 1–16, Sep. 2018, doi: 10.1155/2018/1058170.

[25] M. Pepe, C. Lima, and E. Martinelli, "Early-age properties of concrete based on numerical hydration modelling: A parametric analysis," *Materials*, vol. 13, no. 9, p. 2112, May 2020, doi: 10.3390/ma13092112.

[26] W. M. T. D. Wasala and H. D. Yapa, "Prediction of temperature development in concrete using semi-adiabatic temperature measurements," *Eng.-J. Inst. Eng. Sri Lanka*, vol. 50, no. 3, pp. 1–8, 2017, doi: 10.4038/engineer.v50i3.7261.

[27] S. Wu, D. Huang, F.-B. Lin, H. Zhao, and P. Wang, "Estimation of cracking risk of concrete at early age based on thermal stress analysis," *J. Thermal Anal. Calorimetry*, vol. 105, no. 1, pp. 171–186, Jul. 2011, doi: 10.1007/s10973-011-1512-y.

[28] A. Ilc, G. Turk, F. Kavčič, and G. Trtnik, "New numerical procedure for the prediction of temperature development in early age concrete structures," *Autom. Construct.*, vol. 18, no. 6, pp. 849–855, Oct. 2009, doi: 10.1016/j.autcon.2009.03.009.

[29] G. Trtnik, F. Kavčič, and G. Turk, "The use of artificial neural networks in adiabatic curves modeling," *Autom. Construct.*, vol. 18, no. 1, pp. 10–15, Dec. 2008, doi: 10.1016/j.autcon.2008.04.001.

[30] A. Subasi, A. S. Yilmaz, and H. Binici, "Prediction of early heat of hydration of plain and blended cements using neuro-fuzzy modelling techniques," *Expert Syst. Appl.*, vol. 36, no. 3, pp. 4940–4950, Apr. 2009, doi: 10.1016/j.eswa.2008.06.015.

[31] B. Ji, F. Xie, X. Wang, S. He, and D. Song, "Investigate contribution of multi-microseismic data to rockburst risk prediction using support vector machine with genetic algorithm," *IEEE Access*, vol. 8, pp. 58817–58828, 2020, doi: 10.1109/ACCESS.2020.2982366.

[32] O. Altay, M. Ulas, and K. E. Alyamac, "Prediction of the fresh performance of steel fiber reinforced self-compacting concrete using quadratic SVM and weighted KNN models," *IEEE Access*, vol. 8, pp. 92647–92658, 2020, doi: 10.1109/ACCESS.2020.2994562.

[33] M. Su, Q. Zhong, H. Peng, and S. Li, "Selected machine learning approaches for predicting the interfacial bond strength between FRPs and concrete," *Construct. Building Mater.*, vol. 270, Feb. 2021, Art. no. 121456, doi: 10.1016/j.conbuildmat.2020.121456.

[34] H.-B. Zhao, "Slope reliability analysis using a support vector machine," *Comput. Geotechnics*, vol. 35, no. 3, pp. 459–467, May 2008, doi: 10.1016/j.compgeo.2007.08.002.

[35] P. Samui, "Support vector machine applied to settlement of shallow foundations on cohesionless soils," *Comput. Geotechnics*, vol. 35, no. 3, pp. 419–427, May 2008, doi: 10.1016/j.compgeo.2007.06.014.

[36] A. T. C. Goh and S. H. Goh, "Support vector machines: Their use in geotechnical engineering as illustrated using seismic liquefaction data," *Comput. Geotechnics*, vol. 34, no. 5, pp. 410–421, Sep. 2007, doi: 10.1016/j.compgeo.2007.06.001.

[37] D. Liu, Q. Xu, Y. Tang, and Y. Jian, "Prediction of water inrush in long-lasting shutdown karst tunnels based on the HGWO-SVR model," *IEEE Access*, vol. 9, pp. 6368–6378, 2021, doi: 10.1109/ACCESS.2020.3047626.

[38] W. Qiao, K. Huang, M. Azimi, and S. Han, "A novel hybrid prediction model for hourly gas consumption in supply side based on improved whale optimization algorithm and relevance vector machine," *IEEE Access*, vol. 7, pp. 218–230, 2019, doi: 10.1109/ACCESS.2019.2918156.

[39] W. Caesarendra, A. Widodo, and B.-S. Yang, "Application of relevance vector machine and logistic regression for machine degradation assessment," *Mech. Syst. Signal Process.*, vol. 24, no. 4, pp. 1161–1171, May 2010, doi: 10.1016/j.ymssp.2009.10.011.

[40] L. Wei, Y. Yang, R. M. Nishikawa, M. N. Wernick, and A. Edwards, "Relevance vector machine for automatic detection of clustered microcalcifications," *IEEE Trans. Med. Imag.*, vol. 24, no. 10, pp. 1278–1285, Oct. 2005, doi: 10.1109/TMI.2005.855435.

[41] V. N. Vapnik, "An overview of statistical learning theory," *IEEE Trans. Neural Netw.*, vol. 10, no. 5, pp. 988–999, Sep. 1999, doi: 10.1109/72.788640.

[42] S. M. Clarke, J. H. Griebsch, and T. W. Simpson, "Analysis of support vector regression for approximation of complex engineering analyses," *J. Mech. Des.*, vol. 127, no. 6, pp. 1077–1087, Nov. 2005, doi: 10.1115/1.1897403.

[43] Z. Chen and W. Liu, "An efficient parameter adaptive support vector regression using K-means clustering and chaotic slime mould algorithm," *IEEE Access*, vol. 8, pp. 156851–156862, 2020, doi: 10.1109/ACCESS.2020.3018866.

[44] H. Kim and D. Lee, "A study on the properties of hydration heat of mass concrete using blast-furnace slag cement and fly-ash," *J. Regional Assoc. Architectural Inst. Korea*, vol. 11, no. 4, pp. 291–297, 2009.

[45] X.-Y. Wang, "Simulation of temperature rises in hardening portland cement concrete and fly ash blended concrete," *Mag. Concrete Res.*, vol. 65, no. 15, pp. 930–941, Aug. 2013, doi: 10.1680/macr.13.00019.

[46] X.-Y. Wang, H.-K. Cho, and H.-S. Lee, "Prediction of temperature distribution in concrete incorporating fly ash or slag using a hydration model," *Compos. B, Eng.*, vol. 42, no. 1, pp. 27–40, Jan. 2011, doi: 10.1016/j.compositesb.2010.09.017.

[47] G. Dai, Y. Tang, J. Liang, L. Yang, and Y. F. Chen, "Temperature monitoring of high-speed railway bridges in mountainous areas," *Struct. Eng. Int.*, vol. 28, no. 3, pp. 288–295, Jul. 2018, doi: 10.1080/10168664.2018.1464376.

[48] V. K. R. Kodur, P. P. Bhatt, P. Soroushian, and A. Arablouei, "Temperature and stress development in ultra-high performance concrete during curing," *Construct. Building Mater.*, vol. 122, pp. 63–71, Sep. 2016, doi: 10.1016/j.conbuildmat.2016.06.052.

[49] M. Zhang, X. Yao, J. Guan, and L. Li, "Study on temperature field massive concrete in early age based on temperature influence factor," *Adv. Civil Eng.*, vol. 2020, Oct. 2020, Art. no. 8878974, doi: 10.1155/2020/8878974.

[50] X. Peng and D. Xu, "Projection support vector regression algorithms for data regression," *Knowl.-Based Syst.*, vol. 112, pp. 54–66, Nov. 2016, doi: 10.1016/j.knosys.2016.08.030.

[51] S. Thirukumaran and A. Sumathi, "Enhanced fuzzy C-means clustering with optimization of support vector regression for imputation of medical database," *J. Med. Imag. Health Informat.*, vol. 6, no. 7, pp. 1612–1616, Nov. 2016, doi: 10.1166/jmihi.2016.1859.

[52] W. Qiao and Z. Yang, "Solving large-scale function optimization problem by using a new Metaheuristic algorithm based on quantum dolphin swarm algorithm," *IEEE Access*, vol. 7, pp. 138972–138989, 2019, doi: 10.1109/ACCESS.2019.2942169.

[53] W. Qiao and Z. Yang, "Modified dolphin swarm algorithm based on chaotic maps for solving high-dimensional function optimization problems," *IEEE Access*, vol. 7, pp. 110472–110486, 2019, doi: 10.1109/ACCESS.2019.2931910.

[54] W. Qiao and Z. Yang, "An improved dolphin swarm algorithm based on kernel fuzzy C-means in the application of solving the optimal problems of large-scale function," *IEEE Access*, vol. 8, pp. 2073–2089, 2020, doi: 10.1109/ACCESS.2019.2958456.

[55] W. Qiao, M. Khishe, and S. Ravakhah, "Underwater targets classification using local wavelet acoustic pattern and multi-layer perceptron neural network optimized by modified whale optimization algorithm," *Ocean Eng.*, vol. 219, Jan. 2021, Art. no. 108415, doi: 10.1016/j.oceaneng.2020.108415.

[56] W. Qiao, H. Moayedi, and L. K. Foong, "Nature-inspired hybrid techniques of IWO, DA, ES, GA, and ICA, validated through a k-fold validation process predicting monthly natural gas consumption," *Energy Buildings*, vol. 217, Jun. 2020, Art. no. 110023, doi: 10.1016/j.enbuild.2020.110023.

DUNWEN LIU received the Ph.D. degree in geotechnical engineering from Central South University, Changsha, China, in 2001. From 2003 to 2004, he was a Visiting Scholar with the KTH Royal Institute of Technology, Sweden. He is currently a Professor with the School of Resources and Safety Engineering, Central South University. He has authored over 80 articles published in academic journals. His current research interests include theory and technology of environment friendly rock breaking, prevention, and control of tunnel, and underground engineering disasters. He is an Expert of Hunan Province Safety Production Expert Committee, China. He awards Hunan Province New Century 121 Talent Project, China.

WANMAO ZHANG received the bachelor's degree in city underground space engineering from Southwest Petroleum University, Chengdu, China, in 2020. He is currently pursuing the master's degree with the School of Resources and Safety Engineering, Central South University, China. His current research interests include tunneling and underground engineering and civil engineering safety.

YU TANG received the Ph.D. degree in civil engineering from Central South University, Changsha, China, in 2019. He is currently a Postdoctoral Researcher with the School of Resources and Safety Engineering, Central South University. He presided over one scientific and technological innovation project, Central South University, and one postdoctoral Research Project, China. He has authored 18 articles published in academic journals. His current research interests include method and technology of rock fracturing by high-pressure gas expansion, rock breaking method using thermal shock, and gas expansion coupling effect.

YINGHUA JIAN received the bachelor's degree in mining engineering and the master's degree in engineering mechanics from Central South University, Changsha, China, in 2013 and 2016, respectively, where he is currently pursuing the Ph.D. degree with the School of Resources and Safety Engineering. His current research interests include durability and anticorrosion of concrete.